Studying Vertical Anisotropy of a Horizontally Layered Section Using the Controlled Source Radiomagnetotellurics: an Example from the North-Western Region of Russia

Arseny Shlykov[1], Alexander Saraev[1] and Sudha Agrahari[2]

[1]Institute of the Earth Science, Saint Petersburg State University, Saint Petersburg, Russia
[2]Department of Geology and Geophysics, Indian Institute of Technology, Kharagpur, India

Corresponding author: Arseny Shlykov, a.shlykov@spbu.ru

Abstract

Electrical resistivity anisotropy of rocks has significant influence on measurements and interpretation of electrical and electromagnetic data. Hence, the estimation of anisotropy can provide additional and accurate information about the subsurface. Its negligence during the inversion can lead to erroneous results. Capabilities of the near surface controlled source radiomagnetotelluric (CSRMT) method, which utilizes a horizontal electric dipole (finite length cable) for the estimation of electrical resistivity anisotropy of a horizontally layered subsurface from measurements in the transition zone of the source, are thoroughly discussed in this article. Synthetic modelling studies helped us to determine the parameters for field measurements such as a survey area position near the transmitting cable, its length, transmitter-receiver orientation etc. In addition, a comparison of the synthetic results and the field data, measured over a simple vertically anisotropic 1D geoelectrical section, is done. This exercise facilitates to explain the cause of different sensitivity to the vertical resistivity for different transmitter lengths and Tx-Rx orientation. Synthetic integral sensitivity of impedance for the vertical resistivity of the anisotropic layers is calculated and plotted, which deciphers the area of the maximum sensitivity to the vertical resistivity. This emphasizes that the CSRMT data measured in the transition zone of the cable are affected by the significant impact of both galvanic and inductive modes, which helps in the estimation of macro-scale anisotropy. These data can be used for the purpose of industrial construction, particularly in the selection of appropriate repositories to keep the isolation of the solidified radioactive waste in the Cambrian clays of the North-Western region of Russia. The results of the anisotropic inversion of CSRMT data are also compared with electrical resistivity tomography and hydrogeological data.

Keywords: radiomagnetotellurics, controlled source, horizontal electric dipole, transition zone, anisotropy

1 Introduction

In direct current (DC) sounding methods, such as the vertical electric soundings (VES) or the electrical resistivity tomography (ERT), the primary electric field contains both vertical and horizontal components. Therefore, DC data contains the response of both vertical and horizontal resistivity of rocks. However, for plane wave electromagnetic (EM) sounding methods such as magnetotellurics (MT), the primary electric field in the Earth has the horizontal component and therefore contains response of the horizontal resistivity only. We have similar situation for the inductive transient electro-

magnetic methods (TEM) or for far-field measurements in the controlled source audio-magnetotellurics (CSAMT).

Joint application of DC and EM methods provides the solution of inversion problems with reduced equivalence and also gives the information about anisotropy of rocks. This is possible only because of the different structure of the primary fields of both the methods. Examples of joint inversion of DC and EM data are discussed in (*Raiche et al.*, 1985; *Maler et al.*, 1995; *Meju*, 1996; *Barsukov et al.*, 2004; *Israil et al.*, 2010). Possibilities to estimate the coefficient of anisotropy by the joint inversion of DC and EM data are discussed in *Jupp and Vozoff* (1977), *Christensen* (2000), and *Ivanov et al.* (2011).

Besides pure galvanic and inductive methods, there are several EM methods with the mixed structure of the field. One of these is the CSAMT method with a grounded cable source (*Zonge and Hughes,* 1991). The primary field in the near-field zone of the grounded cable is equivalent to the DC case and contains galvanic mode only. In the far-field zone of the source, the plane wave model is applicable and the field contains the inductive mode only. In the transition zone of the source, the EM field contains significant impact of both the galvanic and inductive modes. This phenomenon is similar to the joint inversion of DC and EM data, which enables the estimation of anisotropy of rocks (*Vanyan*, 1965).

The same possibility to estimate the anisotropy also exists in the controlled-source radiomagnetotelluric (CSRMT) sounding method with the grounded cable – high-frequency analog of the CSAMT method (*Saraev et al.*, 2017). It was demonstrated on synthetic data by *Shlykov and Saraev* (2015).

The account of anisotropy is very important for the reliable electrical and electromagnetic soundings data interpretation. Data on the anisotropy of rocks can be used for the purpose of industrial construction. In the North-Western region of Russia, where enterprises of nuclear industry producing radioactive wastes are located, it is necessary to study the anisotropy of Cambrian and Vendian clays associated with their stratification. The clays are suitable media for the repositories to have the isolation of solidified radioactive wastes. In this connection, it is important to study the anisotropy, connected with diffusion properties of clays. Here, we are presenting a study of the coefficient of anisotropy for a horizontally layered geoelectrical section using both synthetic and real field CSRMT data.

2   *Micro and macro-scale anisotropy*

Sedimentary rocks such as clays or shales are usually characterized by the anisotropy of resistivity caused by grains orientation. In this case the resistivity is different along the layer (horizontal resistivity ρ_h) and across the layer (vertical resistivity ρ_v) with the coefficient of anisotropy $\lambda = (\rho_v / \rho_h)^{1/2}$. This anisotropy caused by the grains orientation and micro structure of sediments is called *micro-scale anisotropy* (*Maillet*, 1947; *Vanyan*, 1965).

The sedimentary section also can contain some stacks of relatively thin layers of different lithology such as the rhythmic alternation of sands and clays or shales with different resistivity values. This is common situation for marine sediments (*Constable*, 2010) but it is not an exotic case on the land. In the resistivity and inductive well logging measurements, these layers are detected as independent elements and the existence of thin layers characterizes the inhomogeneity of the section. Surface based DC or EM soundings have limited resolution and therefore, thin layers cannot be resolved separately. The stack of thin layers will be imaged as a single layer with the anisotropic resistivity characterized by averaged horizontal and vertical resistivities ρ_h and ρ_v. This type of anisotropy, caused due to the alternate sequence of thin layers with different lithology and resistivity, is known as *macro-scale anisotropy* (*Schlumberger et al.*, 1933; *Maillet*, 1947; *Kraev*, 1951; *Vanyan*, 1965).

For one-dimension horizontally layered earth the stack of layers with resistivities ρ_i and thicknesses h_i is equivalent to a single macro-scale anisotropic layer with the following horizontal and vertical resistivity:

$$\rho_h = h_\Sigma \big/ S_\Sigma$$
$$\rho_v = T_\Sigma \big/ h_\Sigma \tag{1}$$

Here $h_\Sigma = \Sigma_i h_i$ – total thickness of the stack, $S_\Sigma = \Sigma_i h_i / \rho_i$ – total longitudinal conductance, $T_\Sigma = \Sigma_i h_i \rho_i$ – total transverse resistance (*Kraev*, 1951; *Keller and Frischknecht*, 1966).

The results of galvanic methods (VES, ERT) depend on both the longitudinal conductance and the transverse resistance of the layers. Resistivity ρ_g and thickness h_g of an isotropic layer is equivalent to an anisotropic one derived by galvanic soundings. They have the following expressions (*Maillet*, 1947; *Kraev*, 1951):

$$h^g = h\sqrt{\rho_v / \rho_h} = h\lambda$$
$$\rho^g = \sqrt{\rho_v \rho_h} \tag{2}$$

In this case, the estimated thickness of equivalent isotropic layer is λ times bigger than the true thickness of initial anisotropic layer and its resistivity is equal to the geometrical mean of horizontal and vertical resistivities of the anisotropic layer. It means that the regular isotropic inversion of VES or ERT data over macro-scale anisotropic medium will lead to the erroneously increased thicknesses directly proportional to the coefficient of anisotropy. Galvanic methods do not allow the determination of the effect of anisotropy themselves without any additional information.

Results of pure inductive methods, such as loop-loop TEM, MT or far-field CSAMT and CSRMT measurements, provide the horizontal resistivity and thickness only. Resistivity ρ^i and thickness h^i of an isotropic layer is equivalent to anisotropic one derived by inductive soundings, and will have the following expressions (*Jupp and Vozoff*, 1977; *Christensen*, 2000; *Ivanov et al.*, 2011):

$$h^i = h$$

$$\rho^i = \rho_h$$

(3)

In this case, the thickness of the equivalent isotropic layer is equal to the thickness of the initial anisotropic layer and its resistivity is equal to the horizontal resistivity. Inductive methods are also not able to determine the effect of anisotropy alone without any additional information, however the thickness can be estimated without an error.

3   The CSRMT method and equipment

In the recent past, several studies were carried out applying the radiomagnetotelluric (RMT) sounding method, which employs the electromagnetic fields of radio transmitters operating in the frequency range from 10 kHz to 1000 kHz (*Tezkan*, 2008). The RMT method does not need an active transmitter due to the use of the EM-field of the existing radio transmitters near the survey area. However, it has a major disadvantage that there exist no radio transmitters below 10 kHz. Therefore, the penetration depth is limited usually up to 30–40 m. In addition, there may not be sufficient number of transmitters if an RMT survey is conducted in a remote location.

An alternative solution is to build own transmitters to create the electromagnetic field instead of using the fields of the existing radio transmitters. This method is called controlled source radiomagnetotellurics (CSRMT). The first works on the development of the CSRMT equipment called Enviro-MT was realized at the University of Uppsala, Sweden (*Bastani*, 2001). The basic purpose was to increase the depth of investigations by changing the limit of the lowest frequency from 10 kHz down to 1 kHz. Two mutually perpendicular and vertical loops (horizontal magnetic dipoles) are used as electromagnetic field sources in the equipment Enviro-MT. Such types of sources have some advantages: array compactness, opportunity of tensor measurements, and the fact that the radiation parameters of the sources (currents in the loadings) do not depend on the earth's resistivity.

However, lack of these sources (limited range of working frequencies 1–12 kHz, small long-range action, no more than 600–800 m, impossibility to use sub harmonics of a basic frequency) limit the prospects of their applications in the CSRMT method. The use of a horizontal electric dipole as a source in the CSRMT method has more advantages. The works on testing this variant have shown an opportunity to realize measurements at significant distances (about 3–4 km) from the source (*Simakov et al.*, 2010; *Tezkan et al.*, 2016; *Saraev et al.*, 2017). Also, the horizontal electric dipole has EM field of the mixed structure with galvanic and inductive modes. These features of the EM field are used in the estimation of anisotropy.

The used equipment RMT-C (*Saraev et al.*, 2017) includes a recorder, electric and magnetic sensors, a transmitter with an electric dipole as a source, and software tools for the data processing and interpretation. The recorder has five channels for synchronous measurements with 16 bits digital ADC in each channel (two electric and three mag-

netic ones). The frequency range of the recorder is 1 kHz – 1000 kHz; the volume of the built-in memory is 8 Gb. The display and keypad of the recorder allow us to work independently in field conditions without an external computer, and the built-in power supply with a resource of 6–8 hours allows measurements during a one working day.

4   Geology of the experimental area

For the field validation of the capabilities of the CSRMT method in the estimation of the anisotropy, we have chosen an area with simple horizontally layered geology and with a macroscale anisotropic layer distribution in the subsurface. This area is located near St. Petersburg, Russia, at the Ulyanovka village. It is in the western side of the Russian Plate and is characterized by the flat structure of the sedimentary cover.

Here, we describe the layers of the geological section from the bottom to the top (*Geology of USSR*, 1971) and their corresponding geoelectrical parameters according to the available borehole data. Additional geological information are derived from the surface exposure of the rocks in the surrounding river canyons.

The base horizon is made up of Lower Cambrian blue clays starting at the depth of about 35–40 m and it's thickness is more than 100–130 m. Assuming high frequencies of CSRMT method (1 kHz and higher), it is not necessary to consider lower horizons because of significantly high thicknesses of the clays. The Lower Cambrian clays have lamellar structure and contain very thin layers (about millimeter or more) of mica and siltstone, and also layers of sandstone with thicknesses from 2 mm to 10 cm (Fig. 1).

The hydrogeological research fulfilled to create repositories for the isolation of solidified radioactive waste indicate that the ratio of horizontal and vertical components of the molecular diffusion coefficient for these clays is about 3–6, and the ratio of horizontal and vertical hydraulic conductivities is about 5–15 (*Pankina et al.*, 2010). Assuming these factors, we can expect that the resistivity of the Lower Cambrian clays in the macro-scale will be anisotropic. We have no a priori information about the resistivity of this layer.
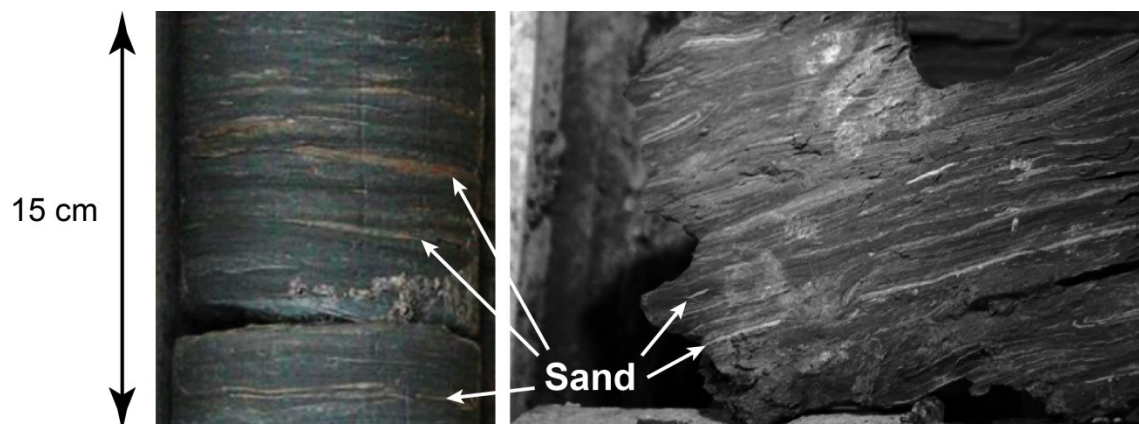

Fig. 1. Lamellar structure of Cambrian clays (*Pankina et al.*, 2010).

The next layer is the Middle Cambrian – Lower Ordovician quartz sands and sandstones. This layer is about 10–15 m thick and relatively homogeneous. Sands lie above the clays with stratigraphic unconformity caused by the Cambrian erosion and this boundary can be wavy. Electrical well logging conducted in the borehole in this area indicates that the sands have resistivity about 150–200 Ωm (Fig. 2).

A thin layer of Ordovician shales (argillites) with thickness of about 0.5–0.8 m is above the sands. This layer is not visible in the electrical well logging data, however, it is detected in the gamma ray logging curve (Fig. 2).
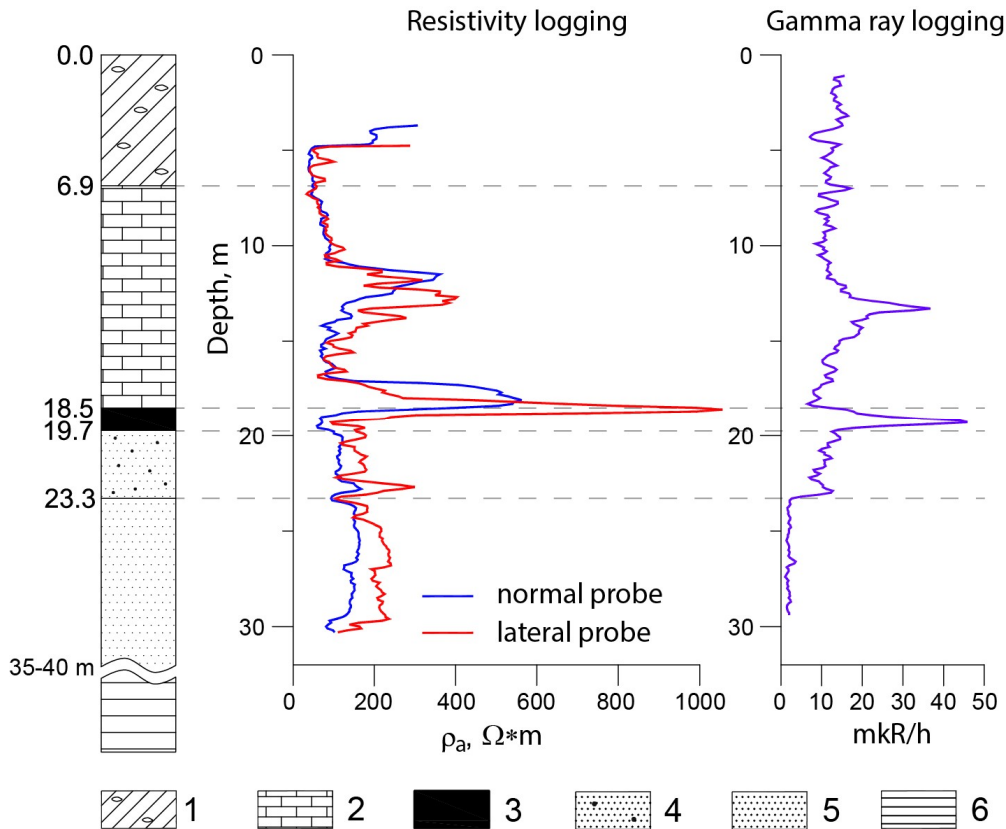

Fig. 2. The lithological column and the electrical and gamma ray well logs in a borehole in the study area. 1 – Quaternary loams, 2 – Ordovician clayey limestones, 3 – Ordovician shales, 4 – Ordovician gray sands, 5 – Cambrian quartz sands, 6 – Cambrian blue clays.

The next layer is a thick stack of different Ordovician limestones. Different sub-layers of limestones contain various amount of clayey portions. More clayey limestone has low resistivity and less clayey one has higher resistivity. The total thickness of the stack of limestones is about 11–13 m. Electrical well logging data clearly indicate that this layer has more and less resistive thin sub-layers. Resistivity of clayey limestones varies from 100 to 1000 Ωm.

In general, the stack of sands, shales and limestones can be integrated into a single anisotropic layer with the thickness of about 32–37 m. Macro-scale anisotropy of this layer is governed by thin layers of conductive shales and alternating layers of high and intermediate resistivity sublayers of limestones. The top layer is the Quaternary glacial loams with pebbles. Its thickness is about 7–10 m.

For the analysis of synthetic CSRMT response from an anisotropic earth, a subsurface model with the following parameters derived from a priori information is considered (Table 1).

Table 1.

Layer's #	ρ_h, Ωm	ρ_v, Ωm	h, m
1	60	60	3
2	30	30	7
3	100	300	25
4	5	50	∞

The first and second layers represent the top and most inhomogeneous Quaternary loams. The third layer is the stack of Cambrian-Ordovician sands, shales and clayey limestones. The fourth layer is Lower Cambrian clays. The resistivity and anisotropy of clays are taken from the literature and hydrogeological data available from the area.

5 Analysis of the synthetic data

Our aim was to estimate the macro-scale anisotropy of the subsurface using the CSRMT method. For this purpose, the methodology was first validated on the synthetic data and after the successful validation it was subsequently applied in the field area. As mentioned above, in–equations 2–3, in case of the pure galvanic or near-field response and the pure inductive or far-field response for the anisotropic layers have simple expressions in comparison with the isotropic equivalents. In the CSRMT method, we have to conduct soundings in the transition zone of the grounded cable for the estimation of the anisotropy (*Shlykov and Saraev*, 2015).

A survey is usually designed in the following manner. The transmitter has a fixed position and the receivers are moved along profiles in the broadside or in-line areas for the measurements of the impedances $Z_{xy} = E_x / H_y$, where X direction coincides with the moment of the transmitter. During the measurements in the transition zone, the distance between the transmitter and the receiver is relatively short in comparison with the length of the transmitter cable. Consequently, the positions of the receivers can be arbitrarily relative to the transmitter in the transition zone. Therefore, the measured total response can contain different impacts of galvanic and inductive modes. This emphasizes the requirement of an in depth analysis of the equivalency of isotropic and anisotropic layers, which helps in the estimation of the importance of including the anisotropy parameters into the inversion for different transmitter-receiver (Tx-Rx) positions.

A schematic representation of the survey layout for synthetic modelling is shown in Figure 3. Four profiles in the broadside direction with Tx-Rx distances from 100 to 250 m, and one profile in the inline direction are considered. Profiles in the broadside area cover only one quadrant because of the symmetry of the primary EM field. Separations between stations along the profiles are 10 m. The synthetic responses consisting of

the apparent resistivity ρ_a and impedance phase φ_Z in the X direction (along the transmitter cable) are calculated at 27 frequencies. These frequencies are 1.5, 2.5, …, 9.5 kHz (subharmonics of 0.5 kHz squared wave signal), 15, 25, …, 95 (subharmonics of 5 kHz) and 150, 250, …, 950 kHz – (subharmonics of 50 kHz). For the interpretation of the data, we used anisotropic controlled-source forward and inversion code described in *Shlykov and Saraev* (2015).
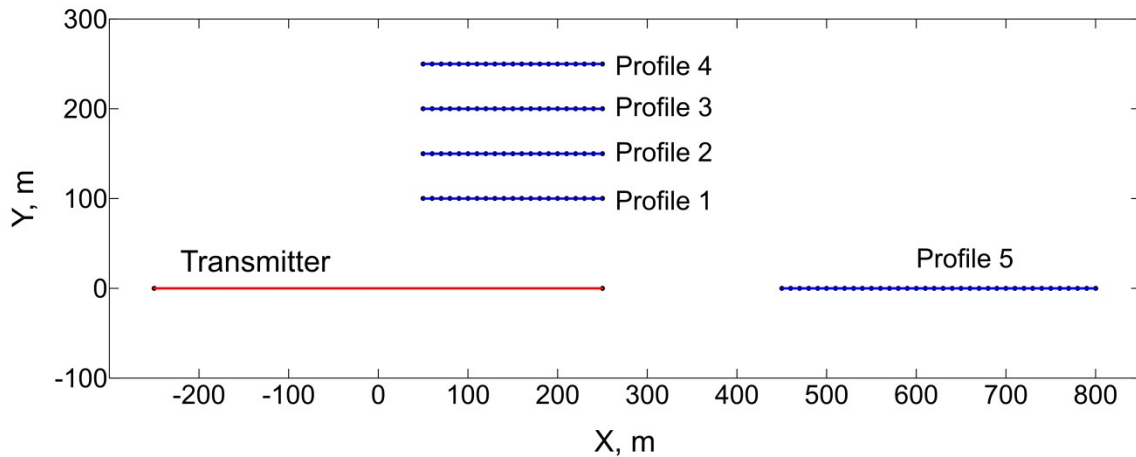

Fig. 3. Schematic arrangement of the synthetic CSRMT survey with a grounded transmitter cable.

In order to estimate the equivalency between the isotropic model and the initial anisotropic model, the regular isotropic inversion of synthetic data was conducted. In inversion, four-layer starting model was used and the regularization was done using the Marquardt method. Isotropic inversion results of the synthetic data, computed for an anisotropic subsurface model, are presented in Figure 4. In all the five profiles, the top two layers are similar to the corresponding layers in the initial model. This is because there is no impact of the galvanic mode in the high frequency far field response.

However, for the broadside measurements, the stations near to the center of the transmitter cable indicate that the resistivity of the models are very close to the horizontal resistivity of the initial model. This shows that very small impacts of the galvanic mode exist in this zone. In the central zone of the profiles from 1 to 4 or in the areas between the center and groundings of the transmitter cable, there exists maximum impact of the galvanic mode. For the profile 1 (closest to the transmitter cable), the transverse resistance of the third layer is similar to the value obtained from the thickness and the vertical resistivity of the initial anisotropic layer. However, other profiles (profiles 2, 3) have less impact of the galvanic mode and therefore, the resistivities of the third and fourth layers tend to be the geometrical mean of the horizontal and vertical resistivities of the corresponding initial anisotropic layers. The transverse resistance of the third layer is equivalent to the value obtained from the thickness and the horizontal resistivity of the corresponding initial anisotropic layer. For the remote profile 4, the resulting model is close to the purely inductive mode, thus the resistivity value of the layer is similar to the horizontal resistivities from initial anisotropic model. This is due to the vanishing impact of the galvanic mode in the far-field zone.
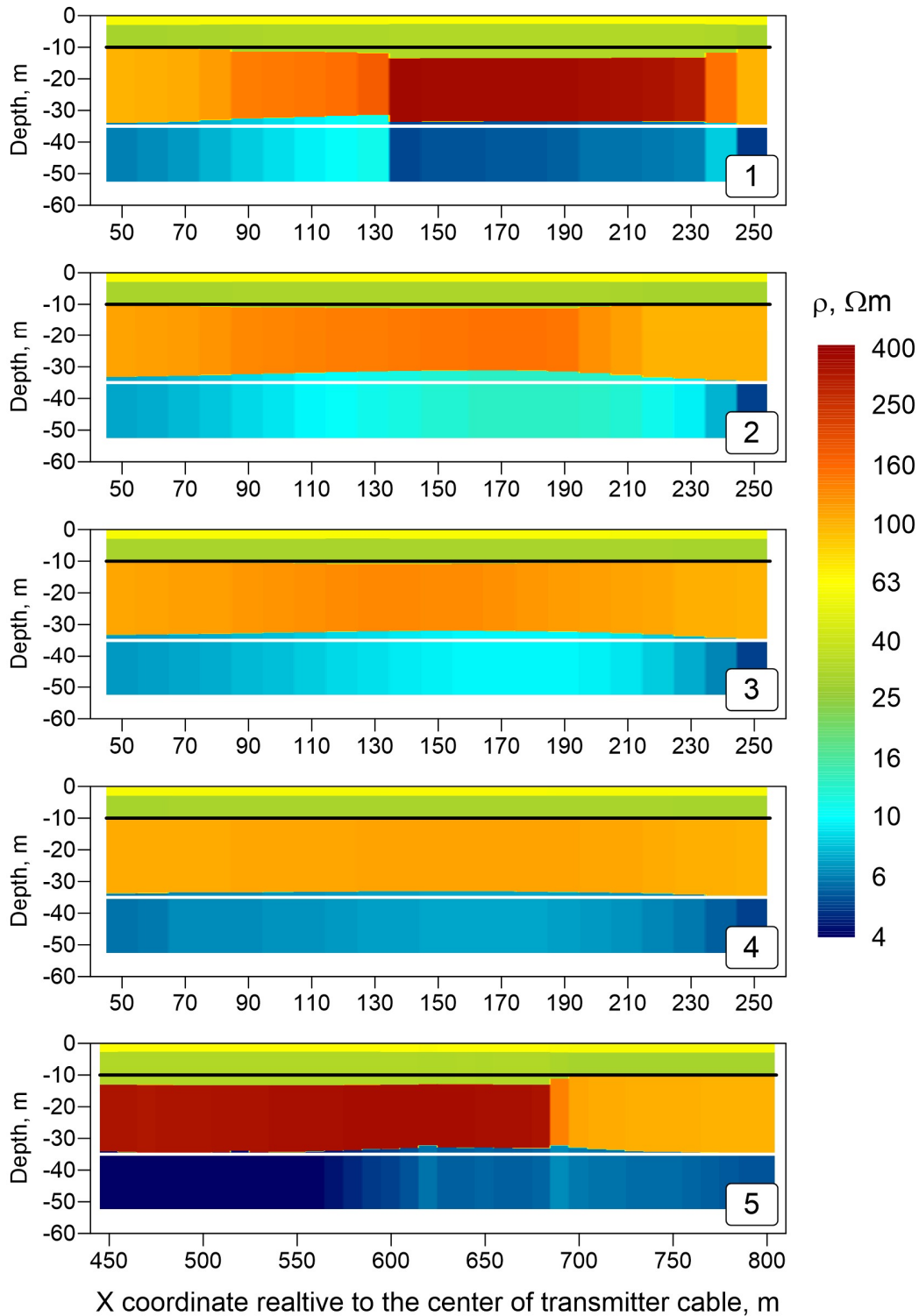
Fig. 4. Results of the isotropic inversion of the transition zone anisotropic CSRMT response. Black line indicates the top boundary of the third layer in the initial anisotropic model, and white line represents the top boundary of the fourth layer in the initial anisotropic model.

In the inline area (profile 5), close to the transmitter, the transverse resistance of the third layer is equal to the corresponding value obtained from the thickness and the vertical resistivity of the initial anisotropic layer. Resistivity of the bottom conductive layer is less than the horizontal resistivity of the initial anisotropic layer. The depth of

the top boundary of this layer is close to corresponding value in the initial model. Going further away from the transmitter, the resistivity of the third layer shows no significant changes while the transition zone effect is significant. Resistivity of the bottom conductive layer is increased up to the horizontal resistivity of the initial anisotropic layer. After the coordinate x=680 m, the EM field meets the plane wave model and the impact of galvanic mode vanishes.

For our case, the synthetic data modelling shows that in the case of transition zone EM response, no increase in the thickness of the isotropic layer equivalent to the anisotropic one is observed. Nevertheless, when we use isotropic inversion for the CSRMT response of anisotropic earth, results of the inversion are highly dependent upon the relative positions of the receiver and the transmitter.

The next step of synthetic analysis is the calculation of the general distribution of the integral sensitivity of the surface impedance Z_{xy} for the vertical resistivity of the anisotropic layers. Following *Zhdanov* (2002), the integral sensitivity is introduced as:

$$S_{int} = \left\{ \sum_f \left[\frac{\partial d_f}{\partial p} \right]^2 \right\}^{\frac{1}{2}}. \qquad (4)$$

where d_f is forward response for frequency f and p is model parameter.

Here, we use following logarithmical transformation of data: $d = ln(\rho_a)$ for apparent resistivity and $d = sign(\varphi_Z)(|\varphi_Z| - 45°)$ for impedance phase. This logarithmic transformation allows us to obtain compatible dynamic range of different responses. Integral sensitivity was calculated using analytical derivatives of kernels (*Shlykov and Saraev*, 2015). Integral sensitivity was calculated for two bottom anisotropic layers only. Also, we simulated EM responses for three different transmitter lengths: 200, 500 and 1000 m cables. We will analyze the unnormalized sensitivity because of better visualization. Calculated integral sensitivity is presented in Figure 5.

Models of the integral sensitivity illustrate two main features of EM field in the transition zone of the cable. First, the sensitivity of the vertical resistivity is maximum in inline area of the transmitter. It is the well-known fact from marine CSEM theory and practice (*Constable*, 2010). It is because of the predominance of the vertical electrical component of primary field in the inline area. Second, the sensitivity to ρ_v in the broadside area depends on the length of the transmitter. For a short transmitter length, the sensitivity in the broadside area is strong and compatible to the sensitivity in the inline area. Increase in the length of the transmitter leads to the decrease in the sensitivity to ρ_v to zero in the broadside area. It has simple physical explanation. Near to groundings, including broadside configuration, the primary field of short cable has strong vertical electrical component in the earth. In case of long grounded cable, the primary field at the center of the cable has only horizontal electrical component in the earth and therefore the sensitivity to ρ_v vanishes.
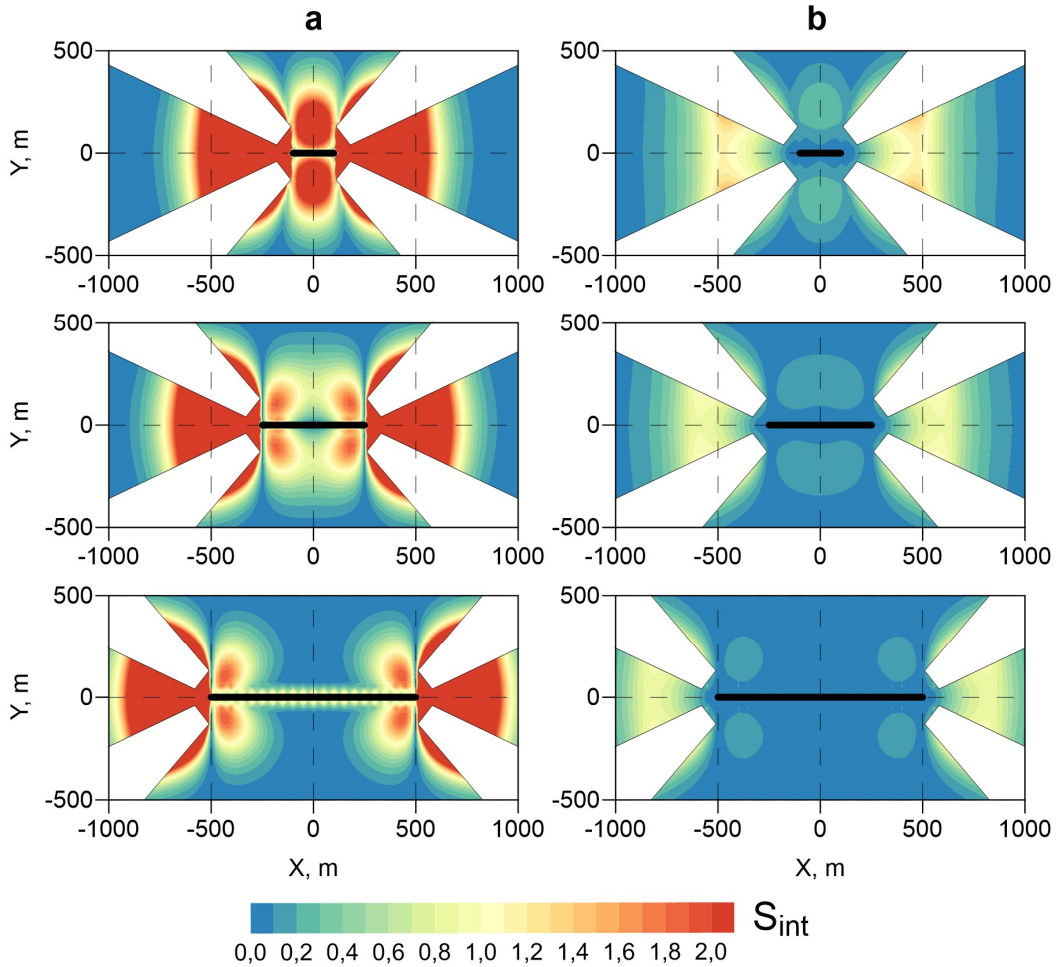
Fig. 5. Synthetic integral sensitivity of impedance Z_{xy} for the vertical resistivity of bottom anisotropic layers in the test model (Table 1) for three different transmitter lengths. Here, a – sensitivity for ρ_{v3}, b – sensitivity for ρ_{v4}. Transmitter marked by solid black lines in the center of map. White polygons mask areas of numerical instabilities because of structure of the cable normal field. In this area, the E_x and H_y fields have near to zero value because of structure of primary field.

6   Results of the field experiments

Field measurements were conducted in two stages with CSRMT measurements in different transmitter-receiver (Tx-Rx) configurations for different lengths of the transmitter cables. At the first stage, two orthogonal 200 m long transmitter cables were used and CSRMT measurements were performed in both broadside and inline areas. At the second stage, CSRMT measurements were made along four profiles in broadside area using 500 m long transmitter cable (as shown in Fig. 3). In this case, one transmitter cable was located close to the profiles for receiving the transition zone response. Another orthogonal transmitter cable was located far from the profiles in the far-field zone for analyzing the transition zone impact. All CSRMT profiles were duplicated by ERT measurements. Full layout is presented in Figure 6.
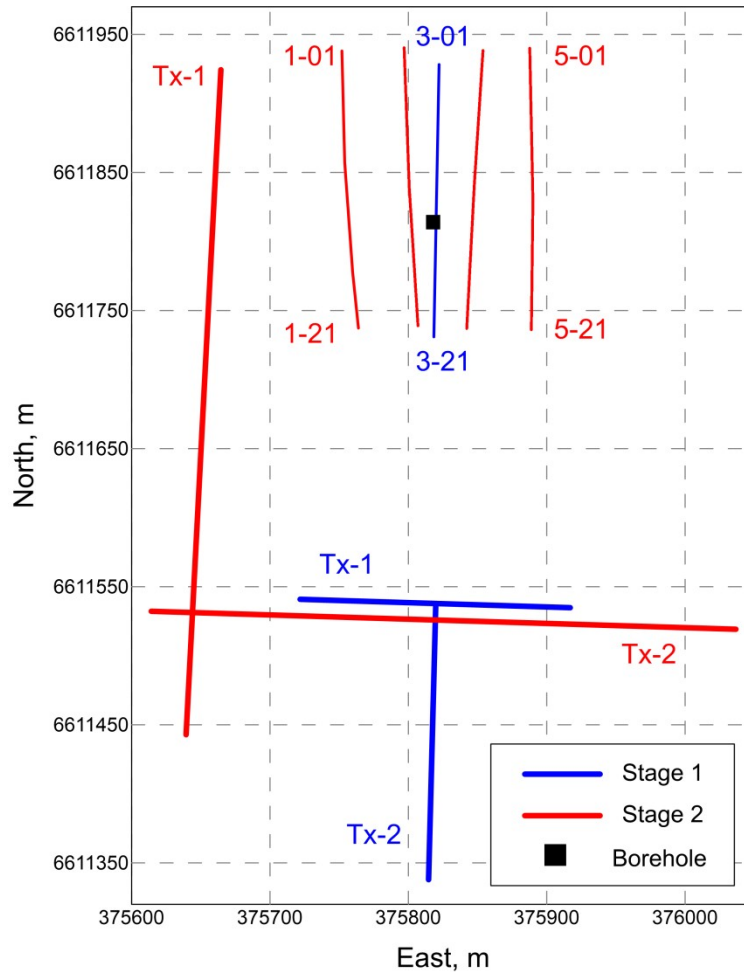
Fig. 6. Layout of the field measurements. Thick red and blue lines indicates the CSRMT transmitters, and the red and blue thin lines represents the profiles of CSRMT and ERT measurements. Numbers on profiles have the format P-SS where P - profile number and SS - CSRMT station number.

The ERT measurements were performed using the pole-dipole forward-reverse array with remote current electrode. Distance between the nearest potential electrodes was 5 m and maximum current electrode offset was 190 m at the first stage and 110 m at the second stage. We used the receiver Medusa (Sib Geophys Pribor, sibgeodevice.ru), the transmitter Astra-100 (Nord-West, nw-geophysics.com) and the programmable electrodes switcher ComDD-2 (Geodevice, geo-device.com). The 2D inversion was performed using the ZondRes2D software (zond-geo.ru). The inverted geoelectrical cross-sections are presented in Figure 7.

The ERT method clearly indicates a three-layer structure of the subsurface. Eastern profiles 4 and 5 have an additional top layer of Quaternary soils, which is very thin with high resistivity value. The thick high resistivity layer in all five cross-sections corresponds to the macro-scale anisotropic stack of Cambrian-Ordovician sands, shales and clayey limestones. Thickness of this layer is 40–45 m and resistivity is about 150–300 Ωm. Interesting feature of the cross-sections in profiles 1 and 2 is the increase (up to 50 m) in the thickness of the high resistivity layer towards the Northern sides of the profiles.
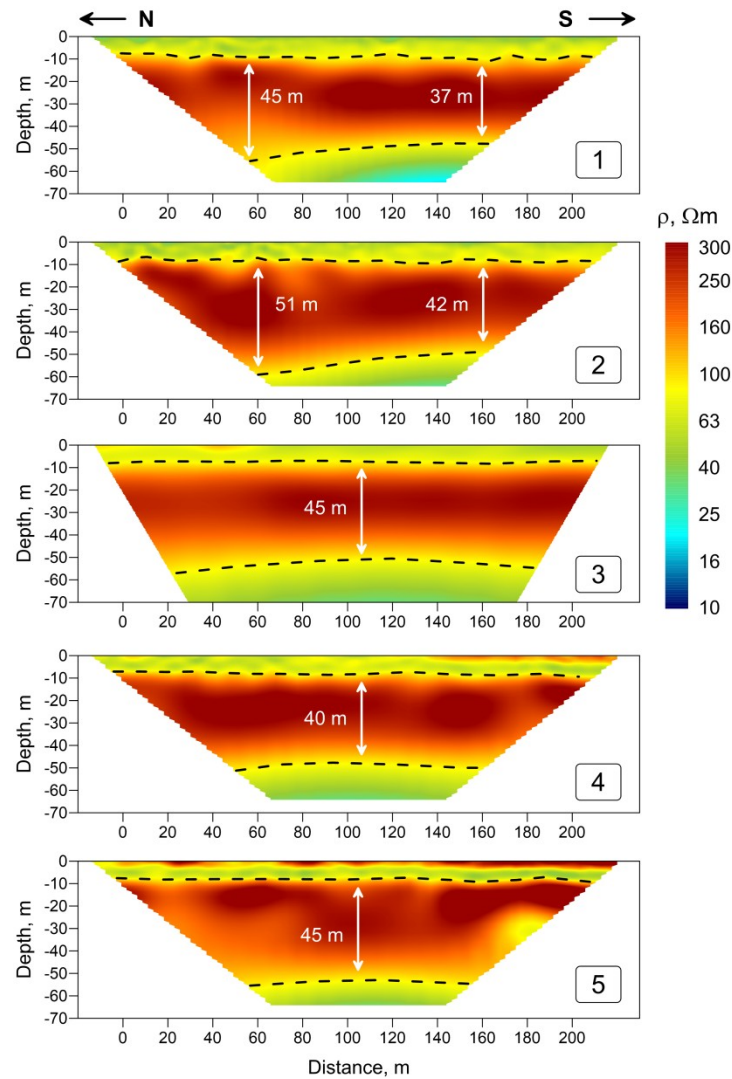
Fig. 7. The 2D inverted sections of the ERT data along five profiles.

For CSRMT field measurements, the local coordinate system has the following orientations: *X* direction points towards the North and *Y* direction to the East (Fig. 6). All CSRMT profiles are 200 m long and the distance between the nearest stations is 10 m. At the first stage, we used two orthogonal 200 m length grounded transmitter cables and conducted measurements along a single profile (number 3 in Fig. 6), in the in-line area of the *X* transmitter, or Tx-2, and in the broadside area of the *Y* transmitter, or Tx-1.

At the second stage, we used two orthogonal transmitter cables of 500 m length and measurements were conducted in broadside areas of both cables. The first transmitter cable in *X* direction was located close to the profiles for receiving the significant transition zone response. Another transmitter in *Y* direction was located far from the profiles to get the far field response. For the estimation of the detectability of the anisotropy with different impacts of the galvanic mode, measurements were conducted along four profiles at different distances from the closest transmitter cable (Fig. 6). In all cases, we measured the vertical magnetic field but the estimated tipper values were highly

distorted (Fig. 8). These distortions cannot be explained with the 1D model therefore the tipper was not used in the inversion.
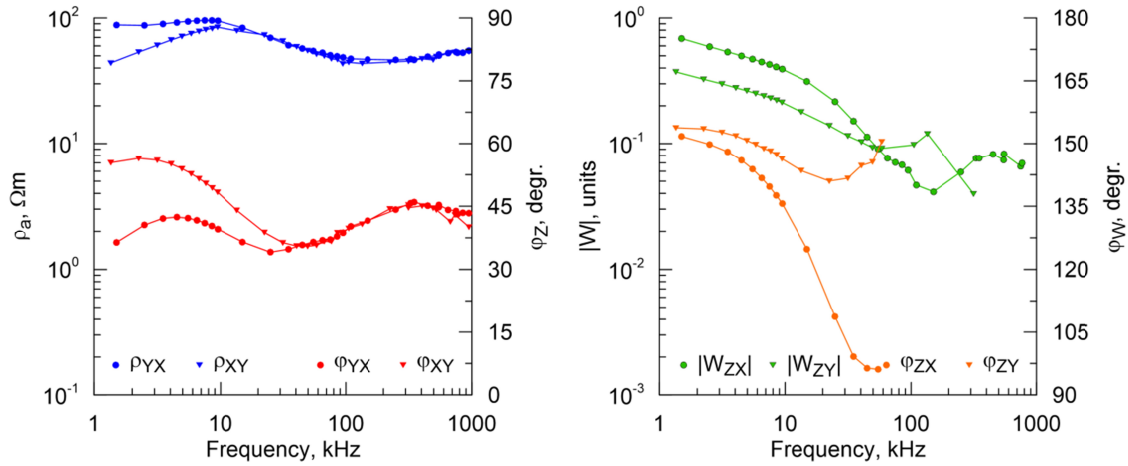

Fig. 8. Sounding curves for the station 3 on the profile 4 measured using 500 m long transmitter cable (red in Fig. 6). Curves of the apparent resistivities and impedance phases in orthogonal directions are converged towards the high frequencies (far-field response). Curves of tipper W_{zx} and W_{zy} are highly distorted at high frequencies and can not be used in the 1D inversion. Here φ_{xy} and φ_{yx} are phases of impedances Z_{xy} and Z_{yx}, and φ_{zx} and φ_{zy} are phases of tippers W_{zx} and W_{zy}.

Results of the 1D anisotropic inversion of CSRMT data obtained at the second stage with relatively long (500 m) cable are presented in Figure 9. In this case, the anisotropic inversion allows us to estimate anisotropy of the third layer only, which corresponds to the stack of limestones, shales and sands. The deeper clay layer is imaged as an isotropic layer with the resistivity in the range of 15–20 Ωm because of the sensitivity of impedance to the vertical resistivity in the broadside area of long cable is very poor (Fig. 5). The third resistive anisotropic layer has the thickness of about 20–25 m, horizontal resistivity of about 100 Ωm, vertical resistivity of about 250 Ωm and coefficient of anisotropy near to 1.4–1.6.

It should be noted that in all profiles, the third layer is resolved as an isotropic layer close to the Northern ends of the profiles (in front of the grounding of the cable) because of the minimum sensitivity to ρ_v in the corresponding area (Fig. 5). In the remote profiles 4 and 5, the third layer is the fragmentary isotropic because of the decreasing impact of the galvanic mode in the far field zone. In profiles 1 and 2, the coefficient of anisotropy slightly increases towards the North.

Black dashed lines in Figure 9 (b), on the cross-sections of the coefficient of anisotropy, correspond to the boundaries of the third resistive layer obtained from the ERT data. The anisotropic inversion results of the CSRMT data are compared with the ERT inversion results. For this purpose, the depth of the bottom boundary of the isotropic equivalent layer for DC case is being calculated using equation (2). Parameters of the third resistive layer were obtained from the anisotropic inversion. This boundary is plotted as magenta lines in Figure 9 (b).
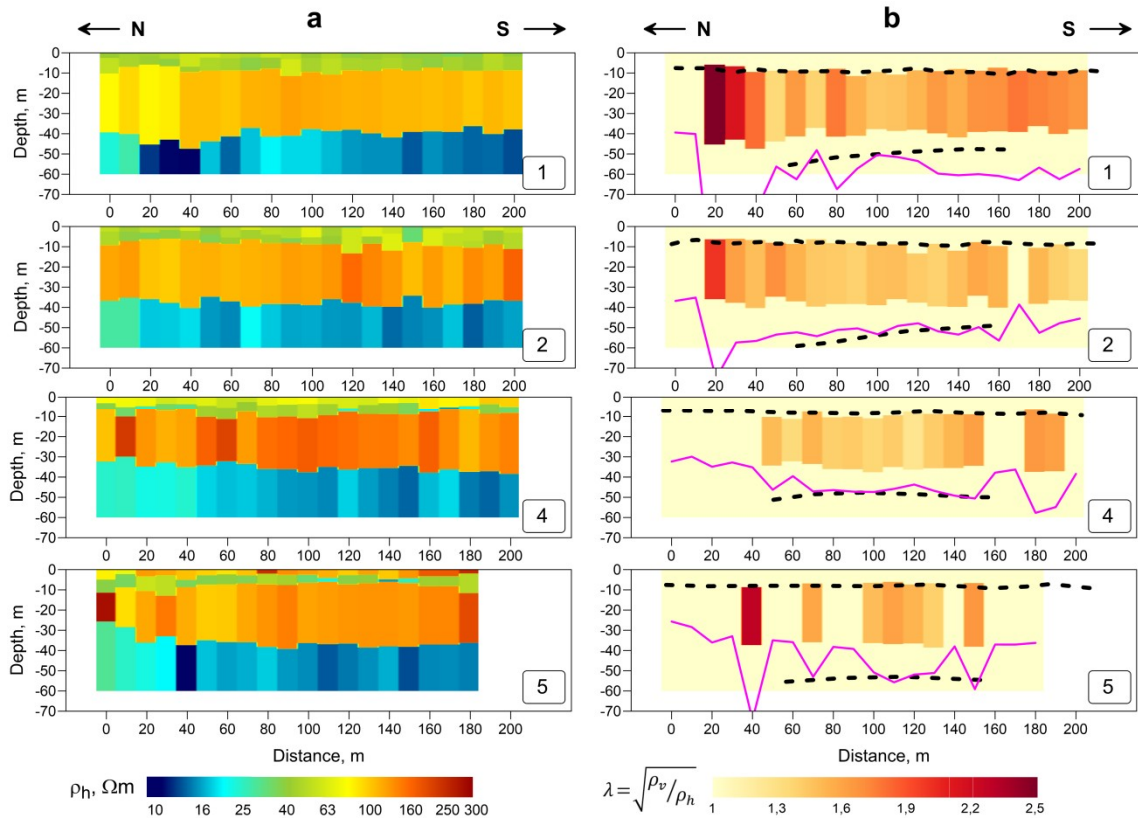
Fig. 9. 1D anisotropic inversion results of CSRMT data measured with 500 m long transmitter cable in Stage 2. Here, the sections in (a) represent the horizontal resistivity, and in (b) infer to the coefficient of anisotropy. Black dashed lines indicate the boundaries of the resistive layers obtained from ERT, and magenta lines show the bottom of the boundary of isotropic equivalent to resistive anisotropic layer obtained from CSRMT and equation (2).

In general, we see that the anisotropy and the thickness of the third layer obtained from CSRMT data are in good agreement with the DC isotropic equivalent according to the equation (2). It is also valid for profiles 1 and 2, where we can observe an increase in the coefficient of anisotropy toward the North and the corresponding increase in the thickness of the resistive layer obtained from the ERT data. Therefore, we can conclude that the anisotropy resolved by CSRMT data is correct and increase in the thickness of resistive layer obtained from the ERT data is apparent, which is due to the increase in the anisotropy coefficient.

Now let's discuss the results obtained at the first stage using short 200 m transmitter cable for the broadside and inline Tx-Rx geometry measured along the profile 3. The results of profile 3 are compared with the results obtained along profile 2, which is located in the close vicinity and measured at the second stage (Fig. 10).

Along these three sections, for the top two conductive layers, no significant difference is observed besides some variation in the thicknesses. Assuming little difference in the location of the two profiles (about 10–20 m), the difference in the thickness of Quaternary loams layer is not so big. In all the three cases, the thickness and the horizontal resistivity of the third resistive layer are compatible. We see little difference in the coefficient of anisotropy. The values of λ_3 varies from 1.6 to1.8 with slight variation

in the lateral direction for the inline measurements with 200 m length transmitter cable. The results for the broadside measurements with 200 m long transmitter cable are similar. However, for the broadside measurements with 500 m long transmitter cable, the λ_3 values are smaller in the range from 1.4 to1.6 with slight variations in the lateral direction.
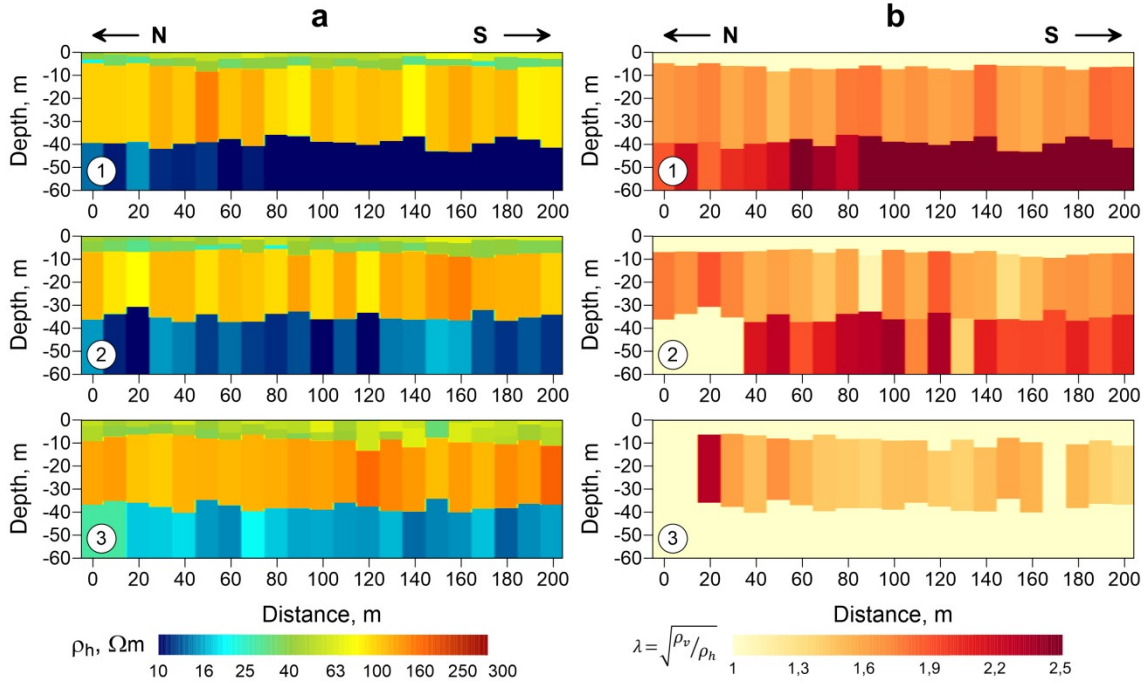

Fig. 10. A comparison of the anisotropic inversion results from CSRMT data obtained using different Tx-Rx geometry and different length of transmitter cables along profiles 2 and 3 (Fig. 6). Here, the sections (a) represents the horizontal resistivity, and (b) the coefficient of anisotropy. The numbers written in the sections are indicative of different arrangements of Tx-Rx geometries. Here, '1' is for 200 m long transmitter cable, inline Tx-Rx geometry, along profile 3; '2' is for 200 m long transmitter cable, broadside Tx-Rx geometry, along profile 3; and '3' is for 500 m length transmitter cable, broadside Tx-Rx geometry, along profile 2.

The most significant difference in the values of the coefficient of anisotropy is observed in the deeper layer of clays. The inline measurements, with 200 m long transmitter cable, contain the strongest impact of the galvanic mode. Therefore, the horizontal resistivity of clays varies from 5 to 7 Ωm and the coefficient of anisotropy λ_4 varies from 2 to 3.5. If we compare the obtained ρ_v/ρ_h for clays from the CSRMT data (squared value for the coefficient of anisotropy) and from the hydrogeological data, we can conclude that these results are similar. As mentioned earlier, the ratio of the horizontal to the vertical hydraulic conductivity of Lower Cambrian clays varies from 5 to 15 (*Pankina et al.*, 2010) and λ_4 (square root of ρ_v/ρ_h) for clays varies from 2 to 3.5 (CSRMT results).

The broadside measurements with 200 m long transmitter cable provide the lower values of the coefficient of anisotropy (2–2.3) and higher horizontal resistivity of clays (10–15 Ωm). The clay layer is resolved as isotropic layer in the northern side of the profile in broadside area because of faster decay in the sensitivity of impedance to the ver-

tical resistivity. Nevertheless, in the broadside area of short transmitter, the sensitivity to ρ_v is still significant and compatible with sensitivity in the inline area. The broadside measurements with 500 m long transmitter cable do not allow us to resolve anisotropy of clays. The horizontal resistivity in this case is higher and close to the values obtained from the ERT data (15–25 Ωm).

Spatial analysis of the integral sensitivity of surface impedance for the vertical resistivity (Figure 5) shows that the layer of clays has to be isotropic and the influence of ρ_v has to be negligible in the last case. It is partly confirmed by the results of the anisotropic inversion of the real field data. But the resistivity of clays is close to the geometrical mean of ρ_h and ρ_v values obtained from the inline measurements (the first case). This means that the vertical resistivity has some influence on the CSRMT data obtained in the transition zone of relatively long transmitter cable. However, the anisotropy is not resolvable in this case. In future, this effect has to be studied in more detail.

7   *Conclusions*

In this paper, we discussed the results of the synthetic modelling and the interpretation of real field data obtained by the ERT and CSRMT methods. The CSRMT data measured in the transition zone of grounded cable contain significant impact of both galvanic and inductive modes, which helps in the estimation of macro-scale anisotropy.

Based on a priori geological and geoelectrical information about the field area, synthetic data were derived for the test site. Using synthetic data, we empirically studied the equivalency of the isotropic and anisotropic layers for different CSRMT transmitter-receiver geometry. It is observed that the results of the regular isotropic inversion of the EM data, obtained over anisotropic media, significantly depend on relative Tx-Rx positions and the impact of the galvanic mode in the primary field of the grounded cable. In case of the broadside measurements, this effect can be described as the equivalency of transverse resistance obtained by thickness and horizontal resistivity of the initial anisotropic layer if the impact of galvanic mode is not so strong. If the impact of galvanic mode is stronger (inline or broadside measurements close to the transmitter cable), this effect can be described as the equivalency of transverse resistance obtained by thickness and vertical resistivity of the initial anisotropic layer. In order to avoid erroneous results in significant anisotropic geoelectrical situations, it is important to consider the anisotropy during the inversion.

The field measurements using the CSRMT method with different Tx-Rx geometry and the comparison of their results with the ERT data allow us to make the following conclusions. In simple geoelectrical situations, it is enough to invert the apparent resistivity and impedance phase only for the estimation of vertical macro-scale anisotropy of resistivity. This parameter is detectible in the inline area of grounded cable and in the broadside area as well (if the transmitter cable is not so long). This fact is illustrated by synthetic modelling and is also verified by the field CSRMT data.

Anisotropy of the intermediate resistive layers is detectible over significant area around the grounded cable including the broadside area. Additionally, the anisotropy of

relatively conductive layers is detectible even below resistive layer for inline and broad-side Tx-Rx setup with relatively short transmitter length. In general, the resolvability of anisotropy can be predicted by synthetic modelling. Anisotropy of the electrical resistivity obtained by CSRMT method is compatible with the hydrogeological data obtained in the laboratory, but this relation has to be studied more carefully and it is the subject of further research.

The study of anisotropy of sedimentary sections is important for the industrial construction, particularly when choosing sites for repositories to have the isolation of solidified radioactive wastes in the Cambrian clays of the North-Western region of Russia. This is due to the fact that the anisotropy is connected with the diffusion properties of clays.

Acknowledgements

References

Barsukov, P.O., E.B. Fainberg and E.O. Khabensky, 2004. Joint inversion of TEM and DC soundings. Abstracts of 10th European meeting of environmental and engineering geophysics «Near surface», Utrecht, The Netherlands, p. 1–4.

Bastani, M., 2001. Enviro-MT – A New Controlled Source/Radio Magnetotelluric System. *Acta Universitatis Upsaliensis*, 179 p.

Christensen, N.B., 2000. Difficulties in determining electrical anisotropy in subsurface investigations. *Geophysical Prospecting*, **48**, 1–19.

Constable, S., 2010. Ten years of marine CSEM for hydrocarbon exploration. *Geophysics*, **75**, 67–81.

Geology of USSR, 1971. Volume 1. Leningrad, Pskov and Novgorod regions. Geological description. "Nedra", 504 p.

Israil, M., Sudha, B. Tezkan, P.K. Gupta, J. Rai, 2010. Joint inversion of TEM and DC resistivity data for mapping the groundwater contamination around Roorkee area, India. Abstracts of 20th EMI Workshop, Giza, Egypt.

Ivanov, P.V., D.A. Alexeev, A.A. Bobachev, P.J. Pushkarev and A.G. Yacovlev, 2011. About complexing the vertical electric soundings and near-field time domain electromagnetic. *Engineer exploration*, **11**, 42–51. In Russian.

Jupp, D.L.B. and K. Vozoff, 1977. Resolving anisotropy in layered media by joint inversion. *Geophysical Prospecting*, **25**, 460–470.

Keller, G.V. and F.C. Frischknecht, 1966. *Electrical Methods in Geophysical Prospecting*. Pergamon Press, Inc. 519 p.

Kraev, A.P., 1951. *Basics of geoelectric*. Part one. Moscow, Leningrad, 445 p. In Russian.

Maillet R., 1947. The fundamental equations of electrical prospecting. *Geophysics*, **12**, 529–556.

Maler, D., H.R. Maurer and A.G. Green, 1995. Joint Inversion of related data sets: DC resistivity and transient electromagnetic soundings. 1-st EEGS Meeting, Expanded Abstracts, p. 461–464.

Meju, M., 1996. Joint inversion of TEM and distorted MT soundings: Some effective practical considerations. *Geophysics*, **61**, 56–65.

Pankina, E.B., V.G. Ruminin, A.M. Nikulenkov, M.P. Glukhova, V.N. Epimakhov, S.G. Mysik, M.N. Baev, V.V. Kobekov and V.F. Degtev, 2010. Anisotropy of clays in diffusion transport of radionuclides. *Radiochemistry*, **52**, 630–637.

Raiche, A.P., D.L.B. Jupp, H. Rutter and K. Vozoff, 1985. The joint use of coincident loop transient electromagnetic and Schlumberger sounding to resolve layered structures. *Geophysics*, **50**, 1618–1627.

Saraev, A., A. Simakov, A. Shlykov and B. Tezkan, 2017. Controlled-source radiomagnetotellurics: A tool for near surface investigations in remote regions. *Journal of App. Geophys*, **146**, 228–237.

Schlumberger, C., M. Schlumberger and E.G. Leonardon, 1933. Some observations concerning electrical measurements. *AIMME Trans*. **110**, 150–182.

Shlykov, A.A. and A.K. Saraev, 2015. Estimation the macroanisotropy of a horizontally layered section from controlled-source radiomagnetotelluric soundings. *Izvestiya, Physics of Solid Earth*, Vol. **51**, No. 4, pp. 583–601.

Simakov, A., A. Saraev, N. Antonov, A. Shlykov and B. Tezkan, 2010. Mobile and controlled source modifications of the radiomagnetotelluric method and prospects of their applications in the near-surface geophysics. IAGA WG 1.2 on Electromagnetic Induction in the Earth. 20th Workshop, Giza, Egypt, September 18–24.

Tezkan, B., 2008. Radiomagnetotellurics. Groundwater geophysics: a tool for hydrogeology. Reinhard Kirsch (ed.), Berlin; Heidelberg: Springer, 295–318.

Tezkan, B., I. Muttaqien and A. Saraev, 2016. 2D Modeling of Controlled Source Radiomagnetotelluric Data Observed on Buried Faults Close to St. Petersburg, Russia. Near Surface Geoscience. Barcelona, Spain, 4–8 September.

Vanyan, L.L., 1965. Basic of electromagnetic soundings. Moscow, Nedra, 108 p. In Russian.

Zhdanov, M.S., 2002. *Geophysical inverse theory and regularization problems*, 1st Edition. Elsevier, USA.

Zonge, K.L. and L.J. Hughes, 1991. Controlled source audio-frequency magnetotellurics. Electromagnetic methods in applied geophysics. V.2 – Applications. Series: Investigations in geophysics, No 3, P. 713–809.